

Dalton Transactions

Accepted Manuscript



This is an *Accepted Manuscript*, which has been through the Royal Society of Chemistry peer review process and has been accepted for publication.

Accepted Manuscripts are published online shortly after acceptance, before technical editing, formatting and proof reading. Using this free service, authors can make their results available to the community, in citable form, before we publish the edited article. We will replace this *Accepted Manuscript* with the edited and formatted *Advance Article* as soon as it is available.

You can find more information about *Accepted Manuscripts* in the [Information for Authors](#).

Please note that technical editing may introduce minor changes to the text and/or graphics, which may alter content. The journal's standard [Terms & Conditions](#) and the [Ethical guidelines](#) still apply. In no event shall the Royal Society of Chemistry be held responsible for any errors or omissions in this *Accepted Manuscript* or any consequences arising from the use of any information it contains.

Photoelectrochemical Property and Its Detection Mechanism of Bi₂WO₆ Nanosheet Modified TiO₂ Nanotube Arrays

Yajun Pang¹, Guangqing Xu^{*1, 2}, Xu Zhang, Jun Lv¹, Kai Shi¹, Pengbo Zhai¹, Qianyun Xue¹,
Xuedong Wang¹, Yucheng Wu^{*1, 2}

1 School of Materials Science and Engineering, Hefei University of Technology, Hefei 230009, China

2 Anhui Provincial Key Laboratory of Advanced Functional Materials and Devices, Hefei University of Technology, Hefei 230009, China.

Abstract:

Bi₂WO₆ nanosheet modified TiO₂ nanotube arrays were synthesized by anodization method combined with sequential chemical bath deposition for enhancing the photoelectrochemical detection performance. Structures, morphologies and elemental compositions of the nanotube arrays were characterized with X-ray diffraction, scanning electron microscope and X-ray photoelectron spectrometer. Bi₂WO₆ nanosheets were successfully deposited on the tube walls of TiO₂ nanotubes. Photoelectrochemical property of the Bi₂WO₆/TiO₂ NTAs was measured with chronoamperometry and cyclic voltammetry using an electrochemical workstation equipped with a UV LED light (365 nm). The optimum detection sensitivity of glucose in water was determined to be 0.244 μA/mM in the linear range of 0 to 2500 μM. Bi₂WO₆ modification on TiO₂ NTAs decreased the background photocurrent and increased the current response to organics at the same time, resulting in the enhancement of photoelectrochemical detection properties. Mechanisms of the Bi₂WO₆ modification are discussed by analyzing the photoelectrochemical process, including optical absorption, charges transfer and surface electrochemical reactions. Direct oxidation by holes rather than indirect oxidation by ·OH radicals is believed to be a key role on this enhancement.

* Corresponding author: Tel.: +86 551 62901372
Email address: gqxu1979@hfut.edu.cn (Guangqing Xu)
ycwu@hfut.edu.cn (Yucheng Wu)

Keywords: TiO₂ nanotube arrays, Bi₂WO₆ nanosheets, photoelectrochemical sensor, organics determination

1 Introduction

TiO₂ is a common used semiconductor nanomaterial possessing many environmental applications including dye-sensitized solar cells [1], water photoelectrolysis [2], biosensors [3], super capacitors [4] and photocatalytic degradation of organics [5] due to its oxidizing ability, nontoxicity, physical and chemical stability. Many efforts have been endeavored on constructing different nanostructures, such as monodispersed nanoparticles [6], nanocrystals in sheet [7], nanotubes [8], nanorods [9] and nanotube arrays [10].

Well aligned TiO₂ nanotube arrays (NTAs) were firstly reported by Grimes and co-workers via anodization of Ti sheet in HF electrolyte [11]. The vertically oriented structures of TiO₂ NTAs become a competing architecture in sensors, such as electrochemical sensor [12], gas sensor [13] and humidity sensor [14] due to the excellent charge transport properties along the nanotubes.

Organic compounds are the commonly existed pollutants with long-term preservation, bioaccumulation and high toxicity, which cannot be naturally degraded. Rapid determination and efficient degradation of organic pollutants in water have become issues of global concern. Chemical oxygen demand (COD) is one of the most used metric in the field of water-quality analysis, and is used frequently as an important index for controlling the operation of wastewater treatment plants. COD determination requires strong oxidants, such as K₂Cr₂O₇ and K₂MnO₄ for complete oxidation of the organics [15, 16], which can be possibly replaced by TiO₂ nanomaterials due to the high oxidizing ability of photogenerated holes.

A photoelectrochemical sensor based on TiO₂ NTAs has been constructed for organics determination, in which the photocurrent increases stepwise with increasing organics concentration [17]. The photoelectrochemical process during the organics determination is very complicated, including optical absorption, charge transfer and surface electrochemical reactions. Many efforts have been endeavored

on TiO₂ NTAs for enhancing the photocatalytic performances or electrochemical activities, such as metal nanoparticles deposition [18], ions doping [19] and semiconductor nanostructures modification [20]. Different metal nanoparticles deposited on TiO₂ NTAs play different roles in the photoelectrochemical behaviors. For example, our previous work [21] reported that Ag nanoparticles decreased the photocurrent, while Pt nanoparticles increased the photocurrent in buffer solution.

Since a low background photocurrent and a high current response to organics are the key factors for enhancing the photoelectrochemical determination performance, it is necessary to control the charges transfer and surface electrochemical reactions, including direct oxidation of organics by holes and indirect oxidation by hydroxyl radicals (OH). It's possible to change the surface electrochemical reactions by modifying the semiconductor photocatalysts on TiO₂ NTAs.

In this study, Bi₂WO₆ nanosheets modified TiO₂ NTAs were designed and constructed to decrease the background photocurrent and increase the current response to organics at the same time. The mechanism of charges transfer and the effect of active species in the photoelectrochemical reactions were deeply discussed.

2 Experimental

2.1 Chemicals and instruments

Titanium foil (99.7%) with a thickness of 0.1 mm was purchased from Beijing Cuibolin Non-Ferrous Technology Developing Co., Ltd. Chemicals, such as ammonium fluoride (NH₄F), ethylene glycol, bismuth nitrate (Bi(NO₃)₃), nitric acid (HNO₃), sodium tungstate (Na₂WO₄), disodium hydrogen phosphate (Na₂HPO₄), sodium dihydrogen phosphate (NaH₂PO₄) and glucose were in analytical reagent grade and purchased from Enterprise Group Chemical Reagent Co., LTD. The supporting electrolyte used in electrochemical measurement was 0.05 M phosphate buffer solution (pH=7) obtained by adjusting the ratio of Na₂HPO₄ to NaH₂PO₄ solutions.

The anodization of Ti foil was conducted in a self-made electrolytic cell with a voltage-stabilized source (DH 1722A-3). The obtained amorphous TiO₂ NTAs were annealed in a muffle furnace (OTF-

1200X) for crystallization. All electrochemical experiments were performed on a CHI660D electrochemistry workstation (Chenhua instrumental Co., LTD., Shanghai, China), comprising three electrodes of an Ag/AgCl (3 M KCl) reference electrode, a platinum wire auxiliary electrode, and a TiO₂ NTAs working electrode (diameter of 10 mm). Photoelectrochemical properties were measured on the workstation equipped with a UV LED spot source with a fixed wavelength of 365 nm and adjustable optical powers from 0 to 1200 mW/cm². The spot diameter of the UV LED is 10 mm and the same as that of the working electrode.

Crystal structures of the samples were characterized by a D/MAX2500V X-ray diffractometer using Cu K α radiation with 2θ ranging from 10 ° to 80 °. Morphologies of the samples were observed with a scanning electron microscope (SEM, SU8020). The elemental components of the sample were determined by an X-ray photoelectron spectrometer (XPS, CALAB250).

2.2 Synthesis

Prior to the anodization, Ti foil was rinsed in ethanol and water successively with ultrasonic vibration for 5 min. Ti foil was put into a two-electrode electrolytic cell as the working electrode, and a graphite electrode was used as the counter electrode. The distance between the two electrodes was 2 cm. Anodic oxidation of Ti foil was performed in an ethylene glycol solution containing 0.15 M NH₄F and 5% H₂O at a voltage of 60 V for 6 h. Then, the obtained TiO₂ NTAs on Ti substrate were washed several times to remove the residual solution. The samples were ultrasonic vibrated in ethylene glycol for 1 min to remove the debris covering on the upper surface of TiO₂ NTAs. The dried TiO₂ NTAs were annealed in a muffle furnace at 500 °C for 2 h to transform the as-prepared amorphous TiO₂ to anatase.

Bi₂WO₆ modification was conducted with a sequential chemical bath deposition method. In a typical procedure, TiO₂ NTAs were sequentially immersed in two ethylene glycol solutions containing 20 mM Bi(NO₃)₃ and 20 mM Na₂WO₄ respectively for 1 min to complete a deposition cycle. And the TiO₂

NTAs should be rinsed with ethanol after each immersion to remove the remanent precursor solution on the surface. The chemical bath deposition cycle was repeated several times to achieve a more deposition amount of Bi_2WO_6 .

2.3 Photoelectrochemical property

Glucose was used as a target organic compound for photoelectrochemical performances measurements and photoelectrochemical sensing. The photoelectrochemical determination of organics was conducted in a flow-injection photoelectrochemical system, composed of a thin-cell photocatalytic reactor, a constant flow pump and an electrochemical workstation. A UV LED spot source with a fixed wavelength of 365 nm, a spot diameter of 10 mm and an adjustable optical power ranging from 0 to 1200 mW/cm^2 was used as the optical source.

Cyclic voltammetry with potentials ranging from 0 to 1 V and a sweeping rate of 10 mV/s was used to characterize the electrochemical activity of the samples in different conditions. Photocurrents of the samples in a phosphate buffer solution were measured with amperometry using an applied potential of 0.2 V. The light was turned on and off with an elapse time of 100 s. The increments of current before and after the UV light illumination gave the photocurrent values. The effect of optical power on photocurrent was evaluated by increasing the optical power outputs step by step.

Photoelectrochemical determination of glucose was performed by amperometric method. Phosphate buffer solution was firstly pumped into the thin cell, and the photocurrent was obtained under UV illumination. After reaching the steady-state current, a glucose solution with fixed concentration was injected into the buffer solution to get an increment of photocurrent. The sensitivity, linear range and detection limit of the determination were calculated by linear fitting the current change with changing glucose concentration.

3 Results and discussions

3.1 Characterizations

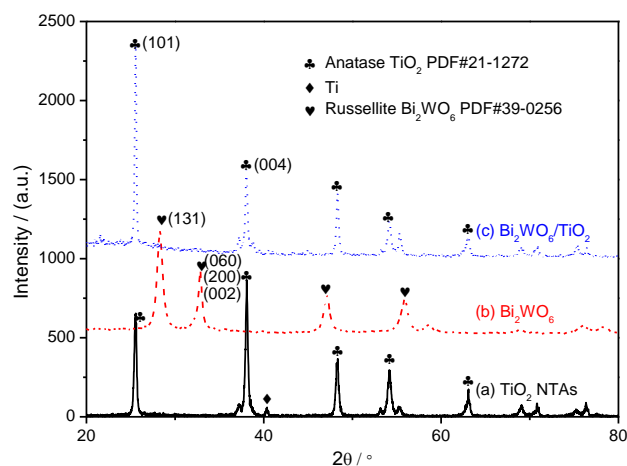
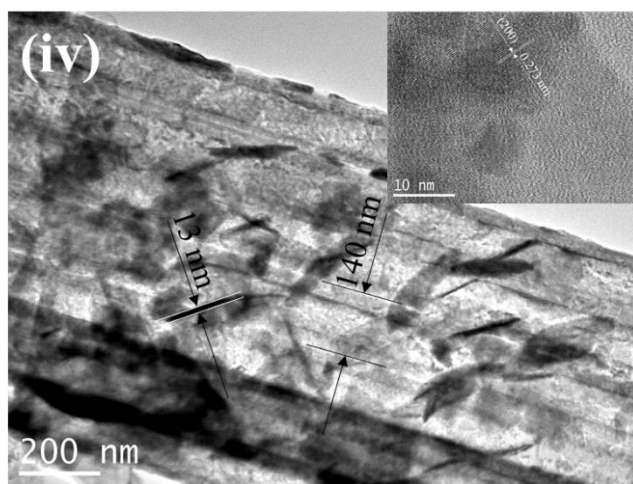
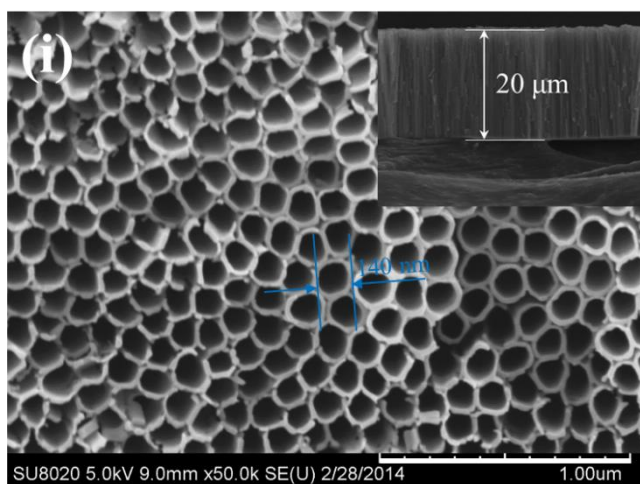


Fig.1 XRD patterns of TiO_2 and $\text{Bi}_2\text{WO}_6/\text{TiO}_2$ NTAs

Fig.1 shows the X-ray diffraction (XRD) patterns of TiO_2 NTAs and $\text{Bi}_2\text{WO}_6/\text{TiO}_2$ NTAs. The structure of as-anodized TiO_2 NTAs is amorphous and becomes anatase after being heat-treated at 500°C for 2 h, as shown by curve (a) in Fig.1. Considering that $\text{Bi}_2\text{WO}_6/\text{TiO}_2$ NTAs are synthesized by sequential chemical bath deposition using $\text{Bi}(\text{NO}_3)_3$ and Na_2WO_4 as the source materials, the XRD pattern of the direct reaction product between $\text{Bi}(\text{NO}_3)_3$ and Na_2WO_4 is Bi_2WO_6 , as shown in curve (b) in Fig.1, which indicates that it is possible to grow Bi_2WO_6 nanocrystals on the tube walls after TiO_2 NTAs being sequentially immersed in the two solutions. Curve (c) in Fig.1 shows the phase structure of TiO_2 NTAs after being deposited with Bi_2WO_6 for 3 cycles. However, no clear diffraction peaks of Bi_2WO_6 can be observed except for that of anatase TiO_2 , which is attributed to the low amount of Bi_2WO_6 on TiO_2 NTAs.



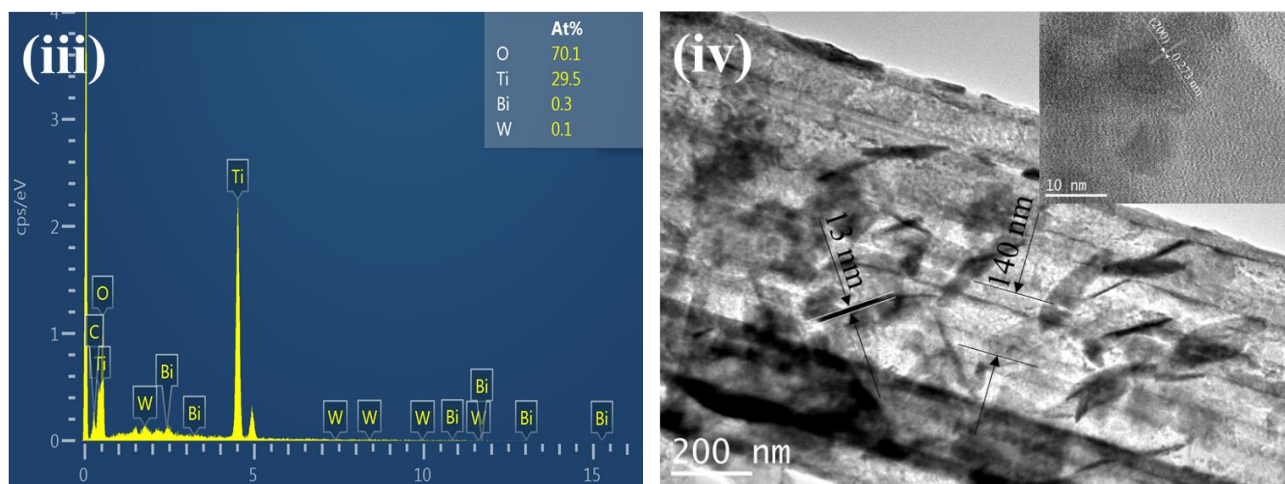


Fig.2 Morphologies of TiO_2 and $\text{Bi}_2\text{WO}_6/\text{TiO}_2$ NTAs, (i) SEM image of TiO_2 NTAs, top-right inset is the profile view; (ii) SEM image of $\text{Bi}_2\text{WO}_6/\text{TiO}_2$ NTAs, top-right inset is the profile view, (iii) EDS pattern of $\text{Bi}_2\text{WO}_6/\text{TiO}_2$ NTAs; (iv) TEM image of $\text{Bi}_2\text{WO}_6/\text{TiO}_2$ NTAs, top-right inset is HRTEM image of $\text{Bi}_2\text{WO}_6/\text{TiO}_2$ NTAs

The morphologies of TiO_2 NTAs before and after being deposited with Bi_2WO_6 nanosheets are shown in Fig.2. Well aligned TiO_2 NTAs can be observed in Fig.2 (i). These nanotubes are tightly aligned with a mean tube diameter of around 140 nm. The top-right inset of Fig.2 (i) shows the profile morphology of as-prepared TiO_2 NTAs, from which the tube length of 20 μm can be observed. Fig.2 (ii) shows the morphology of $\text{Bi}_2\text{WO}_6/\text{TiO}_2$ NTAs. The sequential chemical bath deposition of Bi_2WO_6 possesses no influence on the size and shape of TiO_2 nanotubes. Many small nanosheets can be observed in the tube mouth of TiO_2 nanotubes. Since TiO_2 NTAs were rinsed with ethanol after each immersion in $\text{Bi}(\text{NO}_3)_3$ and Na_2WO_4 solutions, the amount of Bi_2WO_6 is considered to be small and is not enough to cover the tube mouths of TiO_2 nanotubes. The profile morphology of $\text{Bi}_2\text{WO}_6/\text{TiO}_2$ NTAs is shown by the top-right inset in Fig.2 (ii). Some, but not many nanosheets can be observed on the outer wall of TiO_2 nanotubes. Considering that the tight alignment of TiO_2 nanotubes, it is difficult for the solution entering the space among nanotubes during the deposition process. Hence, only few Bi_2WO_6 nanosheets forms on the outer walls of TiO_2 nanotubes. Most of Bi_2WO_6 nanosheets should be deposited on the inner walls of nanotubes, which cannot be observed by SEM. The EDS pattern of

$\text{Bi}_2\text{WO}_6/\text{TiO}_2$ NTAs is shown in Fig.2 (iii). Small peaks of W and Bi can be observed besides the main elements of Ti and O, confirming the existence of W and Bi in the nanotube arrays.

For further investigating the existence of Bi_2WO_6 nanosheets in TiO_2 NTAs, the TEM morphologies of $\text{Bi}_2\text{WO}_6/\text{TiO}_2$ NTAs are shown in Fig.2 (iv). Parallel aligned nanotubes with diameter of approximate 140 nm can be clearly observed. Many nanosheets with thickness of 13 nm can be observed inside or outside of the nanotubes. The HRTEM image of a nanosheet is shown in the top-right inset of Fig.2 (iv). The lattice space is measured to be 0.273 nm, which corresponds to the (200) crystal plane of Bi_2WO_6 (PDF#39-0256), confirming the existence and crystal structure of Bi_2WO_6 nanosheets.

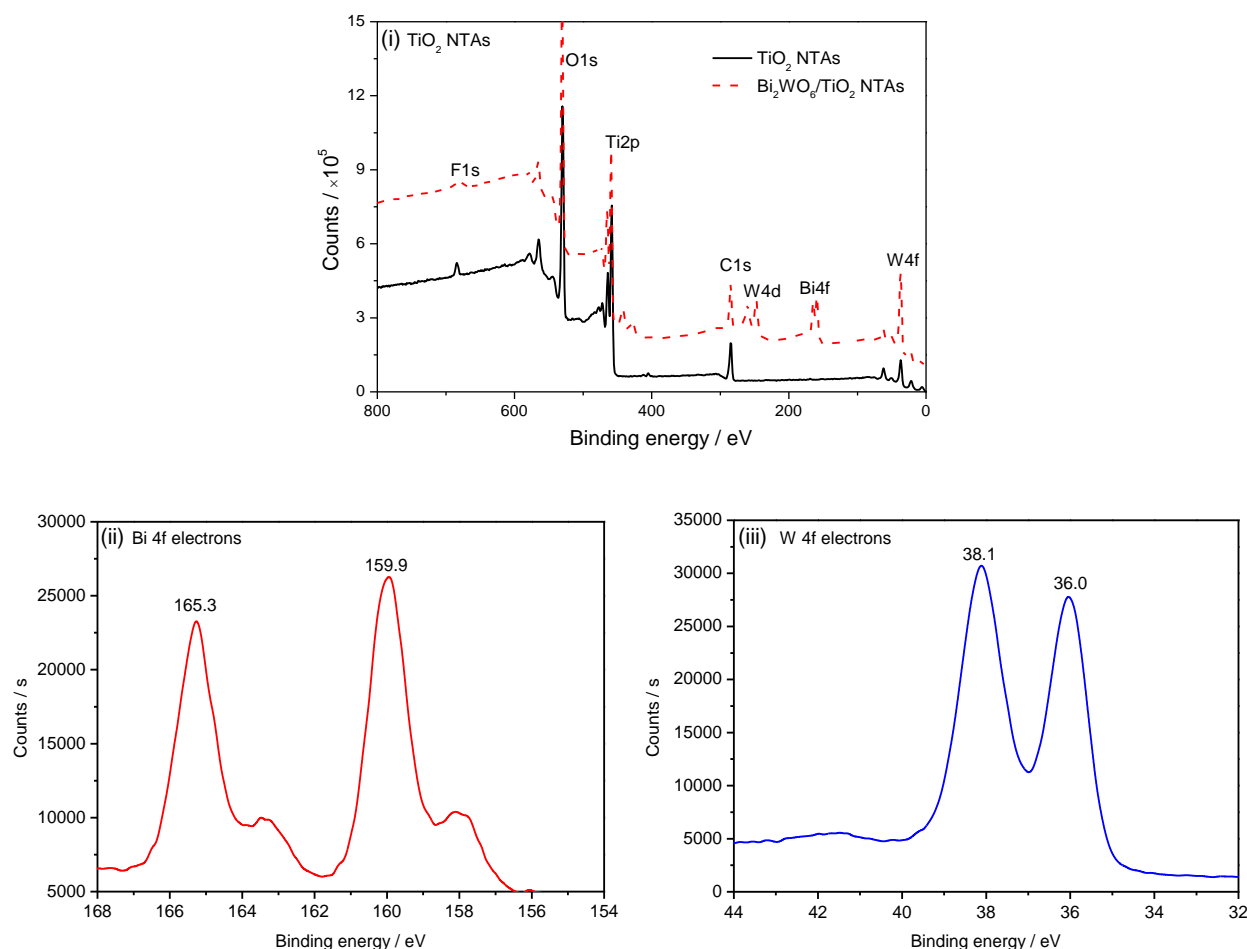


Fig.3 XPS patterns of TiO_2 and $\text{Bi}_2\text{WO}_6/\text{TiO}_2$ NTAs, (i) survey patterns, (ii) Bi 4f electrons, (iii) W 4f electrons

Fig.3 shows the XPS patterns of TiO_2 and $\text{Bi}_2\text{WO}_6/\text{TiO}_2$ NTAs. Fig.3 (i) compares the survey patterns of TiO_2 and $\text{Bi}_2\text{WO}_6/\text{TiO}_2$ NTAs. In both patterns, sharp peaks of O1s at 530.2 eV and Ti 2p at 458.2 eV confirm the major ingredients of the sample. The small peak of F1s at 684.2 eV is due to the residual F^- ions brought in during the anodizing process. Peak of C1s at 284.7 eV, found in both patterns, is originated from the testing process of XPS. Except for the peaks observed in the pattern of TiO_2 NTAs, three additional peaks with binding energies at approximate 38 eV, 164 eV and 260 eV are found in the pattern of $\text{Bi}_2\text{WO}_6/\text{TiO}_2$ NTAs corresponding to W4f, Bi4f and W4d electrons, respectively, which confirms further the existence of W and Bi elements in $\text{Bi}_2\text{WO}_6/\text{TiO}_2$ NTAs.

Fig.3 (ii) shows the XPS peaks of Bi 4f electrons with binding energy ranging from 154 to 168 eV in high resolution. Double peaks with binding energy at 165.3 and 159.9 eV correspond to the 4f 5/2 and 4f 7/2 electron levels of Bi^{3+} ions. The 4f electron levels of W^{6+} ions are composed of two sub-levels with binding energy of 36.0 and 38.1 eV (difference of 2.1 eV), as shown in Fig.3 (iii), corresponding to the 4f 7/2 and 4f 5/2 electron levels of W^{6+} ions.

From the discussion above, Bi_2WO_6 nanosheets modified TiO_2 NTAs can be achieved by sequentially immersing TiO_2 NTAs in the solutions containing $\text{Bi}(\text{NO}_3)_3$ and Na_2WO_4 respectively. The surface of tube walls are the preferred sites for Bi_2WO_6 nanosheets nucleation and growth. This structure can maintain a good contact in the heterojunctions, which is beneficial for the charge transfer during photocatalytic processes. The size of Bi_2WO_6 nanosheets is limited by the size of nanotubes which can only contain a small amount of source solution.

3.2 Photoelectrochemical performance

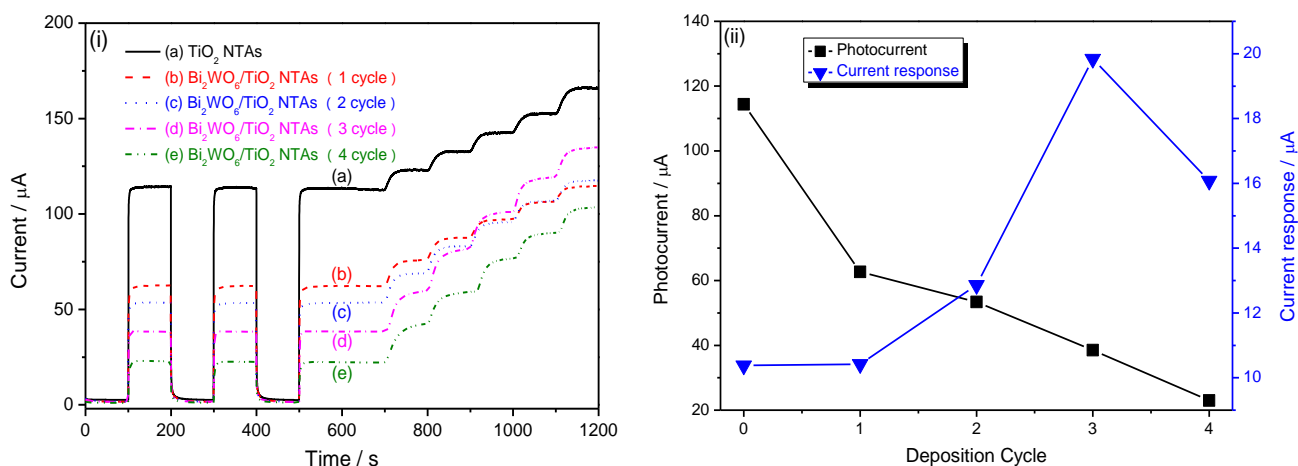


Fig.4 Photocurrents and current responses of TiO₂ and Bi₂WO₆/TiO₂ NTAs with different deposition cycles at the applied potential of 0.2 V, (i) current-time curves, (ii) plots of photocurrent and current response vs. deposition cycle

The photoelectrochemical performance of TiO₂ and Bi₂WO₆/TiO₂ NTAs measured in the thin-cell reactor has been described before [17]. Fig.4 shows the photocurrents and current responses to 0.1 mM glucose of TiO₂ and Bi₂WO₆/TiO₂ NTAs with different deposition cycles at the applied potential of 0.2 V. The change of currents with light off and light on as shown by curve (a) gives the photocurrent produced by TiO₂ NTAs. The current increase to glucose additions reflects the current response. The sharp increase and decrease of current with light on and off indicate the excellent photoelectrochemical activity of TiO₂ NTAs. When glucose is added into the solution, the photocurrent goes up quickly and tends to be stable in 20 s. The photocurrents and current responses of Bi₂WO₆/TiO₂ NTAs to glucose additions is similar to that of TiO₂ NTAs, as shown in curves (b), (c), (d) and (e). Fig.4 (ii) shows the plots of photocurrent and current response vs. Bi₂WO₆ deposition cycle. All photocurrents of Bi₂WO₆/TiO₂ NTAs are lower than that of as-prepared TiO₂ NTAs and decrease with increasing Bi₂WO₆ deposition cycles. However, all the current responses of Bi₂WO₆/TiO₂ NTAs to 0.1 mM glucose are higher than that of TiO₂ NTAs. The current response increases with increasing deposition cycles from 1 to 3 and achieves the maximum of 20 μA with 3 cycles. Large amount of Bi₂WO₆ nanosheets will cover on the top surface of TiO₂ NTAs with the further deposition, which will hinder

the light absorption of TiO_2 NTAs. Low optical absorption efficiency results in low photoelectrochemical performance, of course, both photocurrent and current response decrease with further deposition.

Further deposition decreases the current response due to the hindering effect of large amount nanosheets covered on the top surface.

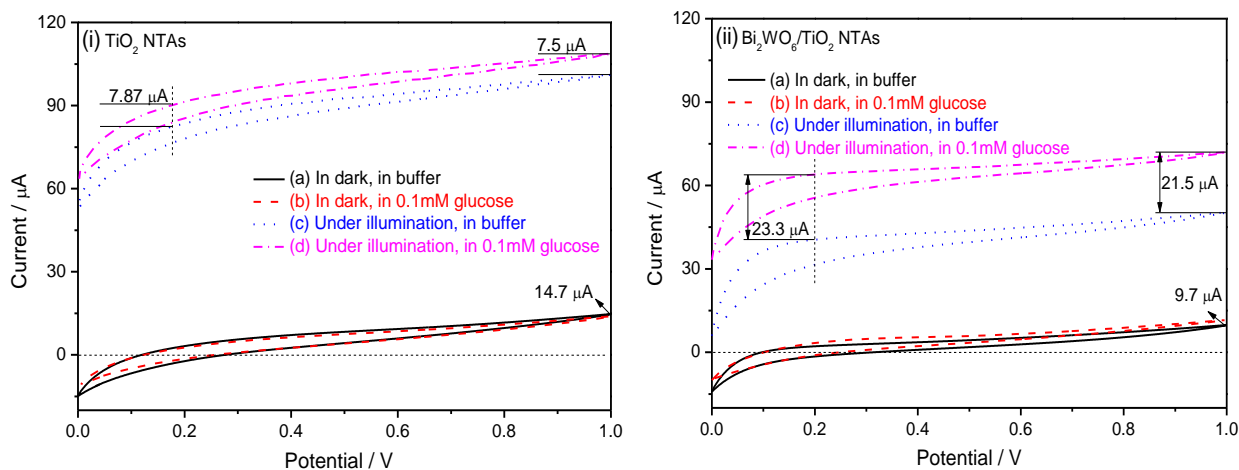


Fig.5 CVs of TiO_2 (i) and $\text{Bi}_2\text{WO}_6/\text{TiO}_2$ (ii) NTAs in different conditions, 3 cycles of Bi_2WO_6 deposition

Fig.5 shows cyclic voltammograms (CVs) of TiO_2 and $\text{Bi}_2\text{WO}_6/\text{TiO}_2$ NTAs in different conditions demonstrating the influence of applied potential on the photocurrent and current response. Fig.5 (i) shows the CVs of as-prepared TiO_2 NTAs in dark and under illumination in the buffer solution without and with 0.1 mM glucose. Curve (a) and curve (b) compare the CVs in the buffer solutions without and with 0.1 mM glucose in dark. The two curves overlap together indicating almost no electrochemical response of TiO_2 NTAs to the added glucose. However, the currents under illumination of UV light increase in the whole potential range, which can be seen from the comparison of curve (a) and curve (c). Increasing applied potential is beneficial for the separation of photo-generated electrons and holes, resulting in the enhancement of the photocurrent. This enhancement is prominent in the potential range of 0 to 0.2 V with photocurrent increasing from 68.5 to 80.2 μA . Further increase of

the potential (from 0.2 to 1 V) only increases the photocurrent from 80.2 to 85 μA . Curve (c) and curve (d) compare the CVs of TiO_2 NTAs under illumination of UV light in buffer and in 0.1 mM glucose solutions respectively. The current responses at different applied potentials are similar with 7.87 μA at 0.2 V and 7.5 μA at 1 V, indicating that the applied potential plays no significant roles on the current response to glucose.

Fig.5 (ii) shows the CVs of $\text{Bi}_2\text{WO}_6/\text{TiO}_2$ TNAs in different conditions. Bi_2WO_6 modification on TiO_2 NTAs changes the CVs greatly. Curve (a) shows the CV of $\text{Bi}_2\text{WO}_6/\text{TiO}_2$ NTAs in the buffer solution in dark, giving that the current of $\text{Bi}_2\text{WO}_6/\text{TiO}_2$ NTAs (9.7 μA at 1 v) is lower than that of TiO_2 NTAs (14.7 μA at 1 V). In consideration that the current in buffer solution originates from the electrochemical water splitting, the decrease of the current indicates a lower electrochemical activity of $\text{Bi}_2\text{WO}_6/\text{TiO}_2$ NTAs in oxygen evolution reaction than that of TiO_2 NTAs. The comparison of curve (b) and curve (a) shows a very little increase of the current in the glucose solution, and the increment is less than 1 μA . Curve (c) shows the CV of $\text{Bi}_2\text{WO}_6/\text{TiO}_2$ NTAs in the buffer solution under UV illumination, which is much lower than that of TiO_2 NTAs in the whole potential range. Although the current of $\text{Bi}_2\text{WO}_6/\text{TiO}_2$ NTAs in the glucose solution under UV illumination is lower than that of TiO_2 NTAs, as shown in curve (d), the current response of $\text{Bi}_2\text{WO}_6/\text{TiO}_2$ NTAs to 0.1 mM glucose (current change between curve (c) and (d)) is higher than that of TiO_2 NTAs. The current responses of $\text{Bi}_2\text{WO}_6/\text{TiO}_2$ NTAs to 0.1 mM glucose are 23.3 μA at 0.2 V and 21.5 μA at 1 V, which are three times higher than of TiO_2 NTAs.

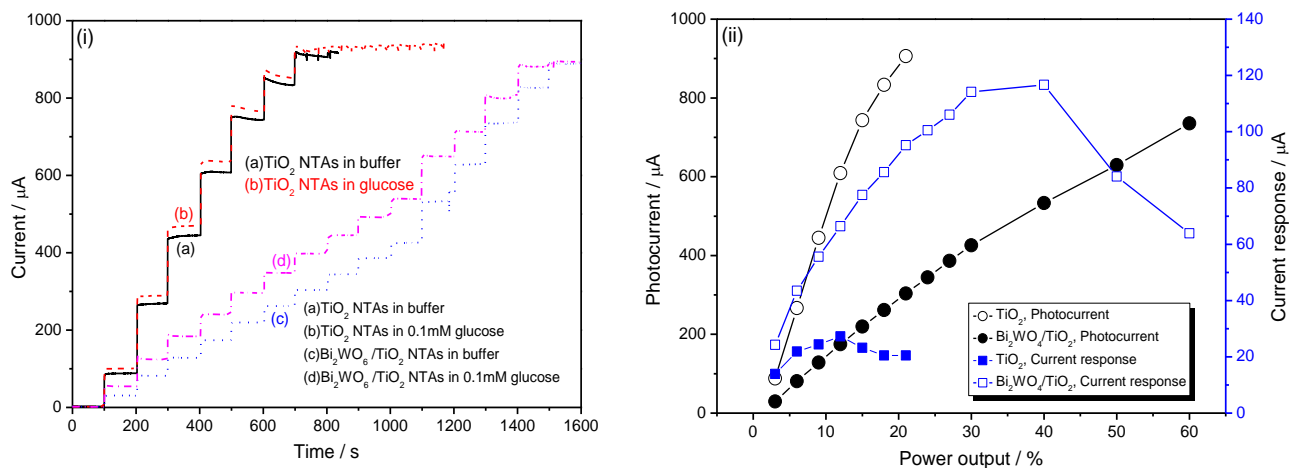


Fig.6 Photocurrents of TiO_2 and $\text{Bi}_2\text{WO}_6/\text{TiO}_2$ NTAs in buffer and 0.1 mM glucose solutions under UV illumination with different power outputs. (i) Current-time curves, (ii) plots of photocurrent and current response vs. power outputs

Fig.6 shows the photocurrents of TiO_2 and $\text{Bi}_2\text{WO}_6/\text{TiO}_2$ NTAs in buffer and 0.1 mM glucose solutions under UV illumination with different power outputs. The maximum optical power is 1200 mW/cm^2 , and can be adjusted by changing the electric powers. The increment of optical power outputs is 3% in the range of 0 to 30%, and is 10% when the outputs are higher than 30%.

Fig.6 (i) shows the current-time curves of TiO_2 and $\text{Bi}_2\text{WO}_6/\text{TiO}_2$ NTAs in different conditions, which can intuitively reflect the relationship between the current response and optical power outputs. As being shown in curve (a), the photocurrent of TiO_2 NTAs goes up step by step with the increase of optical power outputs, indicating the excellent electrochemical activity. However, when the photocurrent reaches $900 \mu\text{A}$, the increase stops with further increasing optical power, which may be due to the limitation of electrochemical reactions on the working electrode and auxiliary electrode. The comparison of curve (b) and curve (a) shows that photocurrent of TiO_2 NTAs in 0.1 mM glucose solution for every steps is higher than that in the buffer solution, the increments give the current response of TiO_2 NTAs to 0.1 mM glucose at different optical powers. Curve (c) and (d) show the current-time curves of $\text{Bi}_2\text{WO}_6/\text{TiO}_2$ NTAs in the buffer solution and 0.1 mM glucose solutions respectively. All the photocurrents of are $\text{Bi}_2\text{WO}_6/\text{TiO}_2$ NTAs lower than that of TiO_2 NTAs under

illumination at the same optical power. And the current responses of $\text{Bi}_2\text{WO}_6/\text{TiO}_2$ NTAs to 0.1 mM glucose obtained from curve (c) and (d) are evidently higher than that of TiO_2 NTAs.

Fig.6 (ii) shows the plots of photocurrent and current response vs. optical power output, from which the variation trends of photocurrent and current response to optical power can be obtained. Both photocurrents of TiO_2 and $\text{Bi}_2\text{WO}_6/\text{TiO}_2$ NTAs are linear to the optical power, especially in the range of low optical powers. The current response firstly increases and then decreases with the increase of optical powers. Current response of TiO_2 NTAs achieves the maximum of $27.3 \mu\text{A}$ at an optical power output of 12%. The current responses of $\text{Bi}_2\text{WO}_6/\text{TiO}_2$ NTAs at all optical powers are higher than that of TiO_2 NTAs, and achieve the maximum of $116.7 \mu\text{A}$ at an optical power of 40%. The current response of $\text{Bi}_2\text{WO}_6/\text{TiO}_2$ NTAs decreases with the further increase of optical power, which may also be due to the limitation of the surface reactions.

3.3 Photoelectrochemical determination

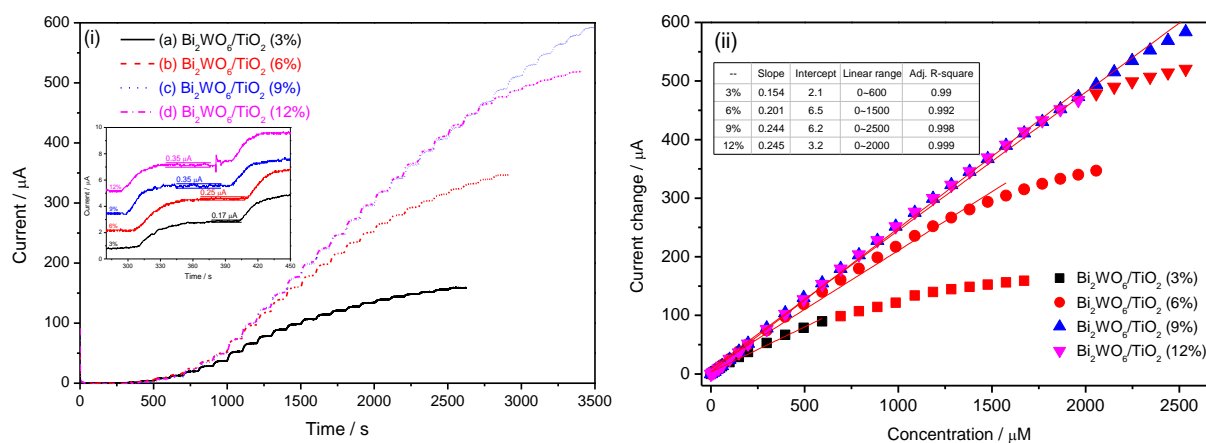


Fig.7 Amperometric response of $\text{Bi}_2\text{WO}_6/\text{TiO}_2$ NTAs to successive additions of glucose (i) and the calibration curve of current change to glucose (ii)

$\text{Bi}_2\text{WO}_6/\text{TiO}_2$ NTAs possess a low background photocurrent and high current response to glucose, both of which are beneficial for enhancing its glucose determination as a photoelectrochemical sensor. Therefore, glucose is also used as target organics for further investigating the determination performance of $\text{Bi}_2\text{WO}_6/\text{TiO}_2$ NTAs photoelectrochemical sensor. The amperometric response of

Bi₂WO₆/TiO₂ NTAs to successive additions of glucose is shown in Fig.7. Fig.7 (i) shows the current-time curves of Bi₂WO₆/TiO₂ NTAs with successive injection of glucose into the solution under the illumination of different optical powers from 3% to 12%. The sequence injections of glucose are 10 μM twice, 20 μM twice, 40 μM once, 50 μM twice and then 100 μM repeated as many times as possible. The real concentration of glucose can be calculated accurately by the changes of glucose and solution volume. The background photocurrents of Bi₂WO₆/TiO₂ NTAs illuminated at different optical powers are much different from each other, which can be obtained from Fig.6. In order to make a convenient comparison, all start points of the current-curves are shifted parallel together. Bi₂WO₆/TiO₂ NTAs possess excellent current responses to glucose injection, and the current increases step by step with each glucose injection. Part of the curves is amplified for checking the current noises of the sample illuminated at different optical powers, as shown by the inset in Fig.7 (i). The current noise increases from 0.17 μA to 0.25 μA, 0.35 μA and 0.35 μA with increasing optical power output from 3% to 6%, 9% and 12%, respectively. High current noise is harmful for the determination performance of the photoelectrochemical sensor.

The calibration plots of current increment vs. glucose concentration are shown in Fig.7 (ii). These plots are linear fitted using the Origin software, which gives the photoelectrochemical parameters of the sensor, such as sensitivity, linear range and detection limit (*dl*). The detection limit (*dl*) of the sensor is calculated by $dl = 3\sigma/m$, where σ is the background current noise, and m is the slope of linear part of the calibration curve. The detection parameters are listed in Tab.1.

Tab.1 Detection parameters of Bi₂WO₆/TiO₂ NTAs with different power outputs

Power output	Current noise (μA)	Sensitivity (μA/μM)	Linear range (μA)	Detection limit (μA)
3%	0.17	0.154	0~600	3.31
6%	0.25	0.201	0~1500	3.73
9%	0.35	0.244	0~2500	4.30

12%	0.35	0.245	0~2000	4.29
-----	------	-------	--------	------

The detection sensitivity (slop) of $\text{Bi}_2\text{WO}_6/\text{TiO}_2$ NTAs (optical power output of 3%) is $0.154 \mu\text{A}/\mu\text{M}$, which is higher than that of TiO_2 NTAs ($0.11 \mu\text{A}/\mu\text{M}$). With the increasing optical power output, the sensitivity increases from 0.154 to 0.201, 0.244 and $0.245 \mu\text{A}/\mu\text{M}$, respectively. Further higher optical power (9%) can achieve a wider linear range of 0 to $2500 \mu\text{M}$, which is much wider than that at the optical power of 3% (linear range of 0 to $600 \mu\text{M}$). The detection limit is calculated to be $4.30 \mu\text{M}$ using the sensitivity of $0.244 \mu\text{A}/\mu\text{M}$ and current noise of $0.35 \mu\text{A}$.

Although a high optical power is beneficial for to get a high sensitivity in organics detection, which can be seen in Fig.6, the influence of high optical power on background photocurrent should also be considered. Macroscopic instability caused by the high background photocurrent is adverse to the photoelectrochemical detection.

3.4 Mechanism discussion

Evidently, Bi_2WO_6 nanosheets modification on TiO_2 NTAs can decrease the background photocurrent in buffer solution and increase the current response to organics, both of which are beneficial for enhancing the photoelectrochemical determination of organics in water. The electronic energy levels of the semiconductors [22] and the schematic diagram of the photoelectrochemical process are shown in Fig.8.

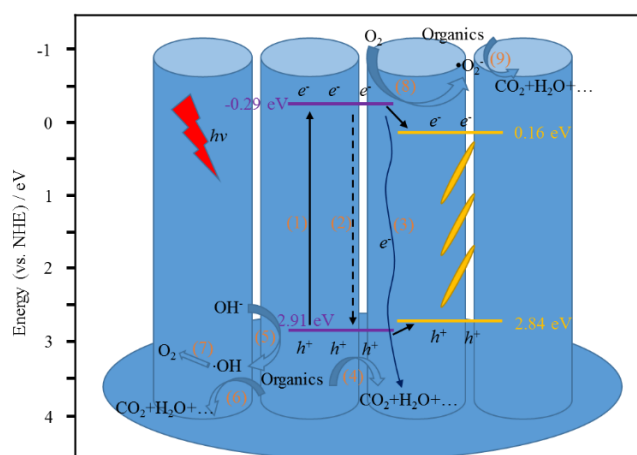


Fig.8 Schematic diagram of the photoelectrochemical process on TiO_2 and $\text{Bi}_2\text{WO}_6/\text{TiO}_2$ NTAs

The photoelectrochemical processes during organics determination are relatively complicated. When TiO_2 NTAs are illuminated by UV light with energy higher than the band gap of TiO_2 , the electrons shift from the valence band (VB) to conduction band (CB) of TiO_2 (process 1), which forms the electron-hole pairs. The recombination of electron-hole pairs (process 2) takes place in a certain chance during the charges transfer process, which is adverse to the photocatalytic and photoelectrochemical performances of TiO_2 TNAs. In photoelectrochemical determination, most electrons transfer to the Ti substrate and form the photocurrent in the external cycle (process 3) driven by the applied potential. The holes transferred to the surface of TiO_2 can oxidize organics to CO_2 , H_2O and other inorganic small molecules directly (process 4). Also the hydroxyl ions (OH^-) can be oxidized to hydroxyl radicals ($\cdot\text{OH}$) by holes (process 5), which possess high oxidizing ability and can degrade organics completely (process 6). Further oxidization of $\cdot\text{OH}$ will produce oxygen evolution (process 7). Part of the CB electrons of TiO_2 will react with dissolve oxygen (process 8), and the product superoxide radicals (O_2^-) possess high oxidization activity to organics (process 9).

The photoelectrochemical determination mechanism of $\text{Bi}_2\text{WO}_6/\text{TiO}_2$ NTAs to organics can be discussed from several aspects, including optical absorption, charge transfer, and surface electrochemical reactions.

3.4.1 Optical absorption

Optical absorption is the first step of the photoelectrochemical determination. High optical absorption efficiency is necessary for enhancing the photocatalytic and photoelectrochemical performances $\text{Bi}_2\text{WO}_6/\text{TiO}_2$ NTAs.

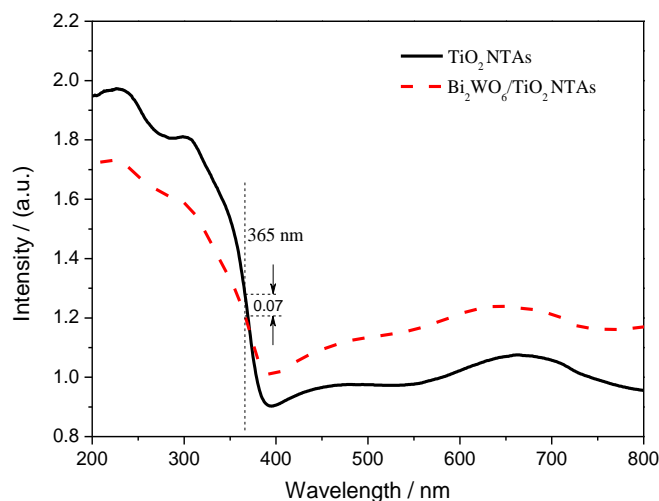


Fig.9 Optical absorption patterns of TiO_2 and $\text{Bi}_2\text{WO}_6/\text{TiO}_2$ NTAs

Fig. 9 shows the optical absorption patterns of TiO_2 and $\text{Bi}_2\text{WO}_6/\text{TiO}_2$ NTAs. TiO_2 NTAs show excellent optical absorption performance in UV region with the absorption edge at about 380 nm, fitting well with the band gap (3.2 eV) of TiO_2 . With Bi_2WO_6 nanosheets deposited on TiO_2 NTAs, the absorption of $\text{Bi}_2\text{WO}_6/\text{TiO}_2$ NTAs in UV region is lower than that of TiO_2 NTAs, and in the visible region is higher than that of TiO_2 NTAs. The light source we used for the photoelectrochemical measurement is a UV LED light with fixed wavelength at 365 nm, therefore, only the absorption performances at 365 nm should be considered for photoelectrochemical determination. The absorption intensity of $\text{Bi}_2\text{WO}_6/\text{TiO}_2$ NTAs at 365 nm is a little lower than that of TiO_2 NTAs. The decrement of the absorption intensity (5.5%) is much lower than the decrement of photocurrent (66.3%, as shown in Fig.4), indicating that the optical absorption is not the main factor for the change of photoelectrochemical performance between $\text{Bi}_2\text{WO}_6/\text{TiO}_2$ NTAs and TiO_2 NTAs.

3.4.2 Electrons transfer

In the photoelectrochemical process, the photogenerated electrons transfer along the nanotubes to Ti substrate forming photocurrent in the external circuit under the role of applied potential. The CB of Bi_2WO_6 is 0.16 eV, and is more positive than that of TiO_2 NTAs. When coupling TiO_2 with Bi_2WO_6 , the photogenerated electrons will flow from CB of TiO_2 to CB of Bi_2WO_6 , and react with dissolved

oxygen to form active O_2^- . This process has little bad effect on the photocatalytic performance of TiO_2 NTAs. However, when used in photoelectrochemical application, Bi_2WO_6 nanosheets as an electron trap block the electron transfer from TiO_2 nanotubes to Ti substrate, resulting in the decrease of photocurrent in buffer solution.

3.4.3 Holes transfer

The photocurrent of TiO_2 NTAs under UV illumination is determined not only by the electrons transfer, but also by holes transfer. The electrons and holes are generated in pairs, and the photocurrent produced by the electrons corresponds to the reaction velocity of holes on the surface of working electrode.

The indirect oxidation of organics by forming OH has no much difference with the direct oxidation by holes in the photocatalytic process. However, there are much difference between those two in the photoelectrochemical process. In the indirect oxidation process (process 5 and 6), the photocurrent signals are controlled by electrochemical reaction of forming OH , resulting in a high background photocurrent. The current response to organics can be obtained by the indirect oxidation of organics which can accelerate OH consumption. The low current response and high background photocurrent are harmful to organics determination. The direct oxidation of organics by holes is an electrochemical process, and the organics concentration can influence the consumption velocity of holes directly, which possess high current response with organics additions.

The photogenerated holes on the surface of TiO_2 nanotubes are easily captured by OH^- ions (process 5) and organics (process 4) in the solution. Many researchers have confirmed that forming OH is the main degradation manner [23]. It's necessary to improve the direct oxidation of organics by holes for enhancing the photoelectrochemical determination. Our previous work [24] has shown that Bi-based nanostructures possess much lower OH concentration than that of TiO_2 nanomaterials, indicating that the direct oxidation by holes is the main manner in photocatalytic process of Bi-based nanostructures.

When Bi_2WO_6 nanosheets with low VB energy are deposited on TiO_2 NTAs, the photogenerated holes will flow from VB of TiO_2 toward VB of Bi_2WO_6 . Low activity of the photocatalytic oxidation of OH^- by the holes on Bi_2WO_6 nanosheets produces high recombination rate between photogenerated electrons and holes, resulting in a low photocurrent in buffer solution. When organics are added in the solution, the direct oxidation of organics by the holes on Bi_2WO_6 nanosheets produces higher current responses than that produced by the indirect oxidation. Therefore, the deposition of Bi_2WO_6 nanosheets on TiO_2 NTAs decreases the background photocurrent and enhances the current response to organics.

In order to confirm the low productivity of $\cdot\text{OH}$ on Bi_2WO_6 nanosheets, $\cdot\text{OH}$ concentrations of TiO_2 and $\text{Bi}_2\text{WO}_6/\text{TiO}_2$ TNAs in the solution during photocatalytic process are compared with terephthalic acid oxidation method. When terephthalic acid solutions containing the photocatalyst are illuminated under UV light, terephthalic acid can react with $\text{HO}\cdot$ and the produced dihydroxy terephthalic acid shows excellent photoluminescence property with an emission peak wavelength at around 420 nm when excited by UV light at 315 nm. The emission peak intensity corresponds to $\cdot\text{OH}$ concentration in the solution. Fig.10 shows the photoluminescence patterns of terephthalic acids containing TiO_2 and $\text{Bi}_2\text{WO}_6/\text{TiO}_2$ NTAs illuminated by UV light. The blank terephthalic acid illuminated by UV light shows no emission, indicating that terephthalic acid is optical inertia. After being illuminated with TiO_2 or $\text{Bi}_2\text{WO}_6/\text{TiO}_2$ NTAs, an emission peak at 420 nm appears due to the produced dihydroxy terephthalic acid by the reaction between terephthalic acid and $\cdot\text{OH}$. The emission intensity of terephthalic acid containing $\text{Bi}_2\text{WO}_6/\text{TiO}_2$ NTAs is much lower than that containing TiO_2 NTAs, indicating a much lower $\cdot\text{OH}$ productivity of $\text{Bi}_2\text{WO}_6/\text{TiO}_2$ NTAs than that of TiO_2 NTAs in the photocatalytic process.

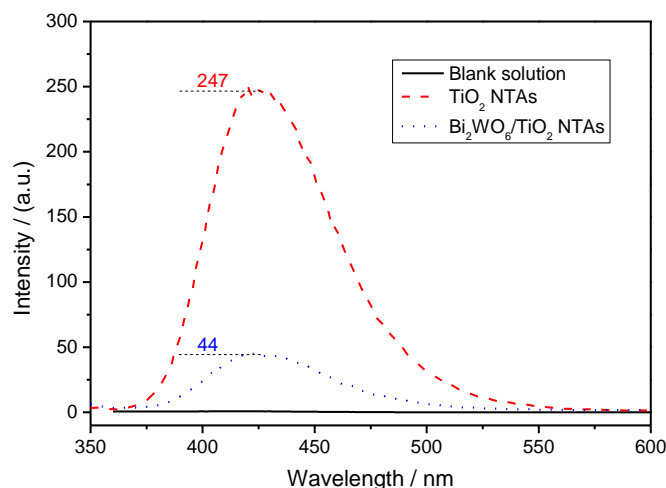


Fig.10 Photoluminescence patterns of terephthalic acids containing TiO_2 and $\text{Bi}_2\text{WO}_6/\text{TiO}_2$ NTAs illuminated by UV light

For further studying the existence of active species during the photoelectrochemical process, trapping agents, such as NaI for h^+ and isopropyl alcohol (IPA) for $\cdot\text{OH}$, were added in the solution. Fig.11 shows the photocurrents of TiO_2 and $\text{Bi}_2\text{WO}_6/\text{TiO}_2$ NTAs in the buffer solution with additions of NaI and IPA respectively. Fig.11 (i) shows the photocurrents of TiO_2 NTAs in the buffer solution with additions of NaI and IPA respectively. The photocurrent of TiO_2 NTAs in blank buffer solution is $100.8 \mu\text{A}$. When NaI is added in the solution, the photocurrent increases a little to $108.8 \mu\text{A}$, indicating that only a small amount of free holes exists in TiO_2 photocatalytic system. When IPA is added in the solution, $\cdot\text{OH}$ radicals are captured by IPA and the reaction rate of forming $\cdot\text{OH}$ radicals is improved. Hence, photocurrent increases from 100.8 to $177.4 \mu\text{A}$. Higher photocurrent increment with IPA than that with NaI indicates that the indirect oxidation by $\cdot\text{OH}$ radicals is the main manner in the photoelectrochemical reactions on TiO_2 NTAs.

The photocurrent of $\text{Bi}_2\text{WO}_6/\text{TiO}_2$ NTAs is much different from that of TiO_2 NTAs. The photocurrent of $\text{Bi}_2\text{WO}_6/\text{TiO}_2$ NTAs in blank buffer solution is only $49.5 \mu\text{A}$, indicating low water splitting activities. The photocurrent in 10 mM NaI solution is $136.2 \mu\text{A}$, which is much higher than that in blank buffer solution ($49.5 \mu\text{A}$), indicating that direct oxidation by holes plays a key role in the photoelectrochemical oxidation process. The photocurrent in 10 mM IPA solution, increases from

49.5 to 87.3 μA . The increment is lower than that in 10 mM NaI solution, indicating that in $\text{Bi}_2\text{WO}_6/\text{TiO}_2$ NTAs photoelectrochemical system the direct oxidation rate by holes is higher than the indirect oxidation rate by forming $\cdot\text{OH}$ radicals. This result is consistent with that of photoluminescence patterns in Fig.10, demonstrating that low $\cdot\text{OH}$ concentration during the photoelectrochemical process is a key factor for enhancing the photoelectrochemical determination performance.

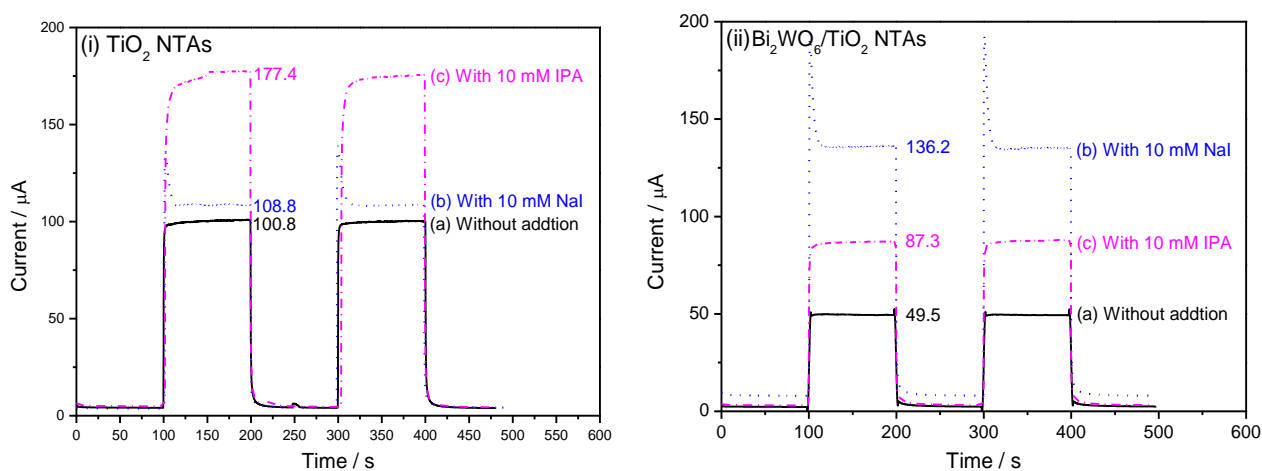


Fig.11 Photocurrents of TiO_2 (i) and $\text{Bi}_2\text{WO}_6/\text{TiO}_2$ (ii) NTAs in the buffer solutions with additions of NaI and IPA respectively

4 Conclusions

Bi_2WO_6 nanosheets are successfully deposited on TiO_2 NTAs by sequential chemical bath deposition. The photoelectrochemical determination performance is improved by decreasing the background photocurrent and increasing the current response at the same time. $\text{Bi}_2\text{WO}_6/\text{TiO}_2$ NTAs photoelectrochemical sensor achieves the optimum detection sensitivity of 0.244 $\mu\text{A}/\text{mM}$, a linear range of 0 to 2500 μM and a detection limit of 4.3 μM . The optical absorption change caused by Bi_2WO_6 deposition is not the reason for the improvement of photoelectrochemical performance. The charges transfer and surface electrochemical reactions play key roles on the photoelectrochemical determination. Electrons transfer from CB of TiO_2 to CB of Bi_2WO_6 decreases the photocurrent caused by the electrons transfer from TiO_2 to the Ti substrate. The holes on Bi_2WO_6 nanosheets transferred

from TiO₂ possess low reaction activity of forming ·OH radicals and high activity of direct oxidation of organics. The photoelectrochemical reactions on the surfaces of TiO₂ and Bi₂WO₆/TiO₂ NTAs are confirmed by terephthalic acid oxidation method with additions of trapping agents of NaI and IPA.

Acknowledgements

This work was supported by Nature Science Foundation of China (51102071, 51172059 and 51272063), Fundamental Research Funds for the Central Universities (2013HGQC0005), and Nature Science Foundation of Anhui Province (1408085QE86).

References

- [1] G.K. Mor, K. Shankar, M. Paulose, O.K. Varghese, C.A. Grimes, *Nano Letter*, 2006, 6, 215-218.
- [2] J.H. Park, S. Kim, A.J. Bard, *Nano Letter*, 2006, 6, 24-28.
- [3] K.S. Mun, S.D. Alvarez, W.Y. Choi, M.J. Sailor, *Acs Nano*, 2010, 4, 2070-2076.
- [4] X. Lu, G. Wang, T. Zhai, M. Yu, J. Gan, Y. Tong, Y. Li, *Nano letters*, 2012, 12, 1690-1696.
- [5] Y. Kuwahara, H. Yamashita, *Journal of Materials Chemistry*, 2011, 21, 2407-2416.
- [6] G. Oskam, A. Nellore, R.L. Penn, P.C. Searson, *The Journal of Physical Chemistry B*, 2003, 107, 1734-1738.
- [7] Z. Lu, M. Ye, N. Li, W. Zhong, Y. Yin, *Angewandte Chemie*, 2010, 122, 1906-1910.
- [8] A. Ghicov, J.M. Macak, H. Tsuchiya, J. Kunze, V. Haeublein, L. Frey, P. Schmuki, *Nano Letters*, 2006, 6, 1080-1082.
- [9] X.L. Li, Q. Peng, J.X. Yi, X. Wang, Y. Li, *Chemistry-A European Journal*, 2006, 12, 2383-2391.
- [10] M. Paulose, K. Shankar, S. Yoriya, H.E. Prakasham, O.K. Varghese, G.K. Mor, C.A. Grimes, *The Journal of Physical Chemistry B*, 2006, 110, 16179-16184.
- [11] D. Gong, C.A. Grimes, O.K. Varghese, W. Hu, R.S. Singh, Z. Chen, E.C. Dickey, *Journal of Materials Research*, 2001, 16, 3331-3334.
- [12] Q. Zheng, B. Zhou, J. Bai, L. Li, Z. Jin, J. Zhang, J. Li, Y. Liu, W. Cai, X. Zhu, *Advanced Materials*, 2008, 20, 1044-1049.
- [13] H.F. Lu, F. Li, G. Liu, Z.G. Chen, D.W. Wang, H.T. Fang, G.Q. Lu, Z.H. Jiang, H.M.

Cheng, *Nanotechnology*, 2008, 19, 3080-3090.

[14] Q. Wang, Y.Z. Pan, S.S. Huang, S.T. Ren, P. Li, J.J. Li, *Nanotechnology*, 2011, 22, 25501-25511.

[15] Y. Han, J. Qiu, Y. Miao, J. Han, S. Zhang, H. Zhang, H. Zhao, *Analytical Methods*, 2011, 3, 2003-2009.

[16] S. Ai, J. Li, Y. Yang, M. Gao, Z. Pan, L. Jin, *Analytica chimica acta*, 2004, 509, 237-241.

[17] C.X. Feng, G.Q. Xu, H.P. Liu, J. Lv, Z.X. Zheng, Y.C. Wu, *Journal of The Electrochemical Society*, 2014, 161, H57-H61.

[18] J. Yu, G. Dai, B. Huang, *The Journal of Physical Chemistry C*, 2009, 113, 16394-16401.

[19] J.H. Park, S. Kim, A.J. Bard, *Nano letters*, 2006, 6, 24-28.

[20] F.X. Xiao, *ACS applied materials & interfaces*, 2012, 4, 7055-7063.

[21] G.Q. Xu, H.P. Liu, J.W. Wang, J. Lv, Z.X. Zheng, Y.C. Wu, *Electrochimica Acta*, 2014, 121, 194-202.

[23] Y. Xu, M.A.A. Schoonen, *American Mineralogist*, 2000, 85, 543-556.

[23] V. Diesen, M. Jonsson, *The Journal of Physical Chemistry C*, 2014, 118, 10083-10087.

[24] J.J. Hu, G.Q. Xu, J.W. Wang, J. Lv, X.Y. Zhang, T. Xie, Z.X. Zheng, Y.C. Wu, *Dalton Transactions*, 2015, 44, 5386-5395.

